

Reduced radiative emission for wide nonpolar III-nitride quantum wells

Philipp Farr, Philipp Horenburg, Heiko Bremers, Uwe Rossow, and Andreas Hangleiter*

Institute of Applied Physics and Laboratory for Emerging Nanometrology, Technische Universität Braunschweig, 38106 Braunschweig, Germany

(Received 8 November 2018; revised manuscript received 17 May 2019; published 29 May 2019)

The radiative rate of GaInN/GaN quantum well structures on nonpolar substrates is investigated for different quantum well widths, showing a significant decrease of the radiative emission towards larger well widths. This effect can be explained by the strict selection rules that apply for radiative transitions in nonpolar structures without any polarization fields in the direction of quantization. The selection rule $\Delta n = 0$ reduces the number of possible radiative transitions that involve higher quantized hole states. These states will get occupied towards room temperature for wider quantum wells due to the decrease in quantization energies. Since the effective masses are strongly different in the conduction and valence bands, the thermal population of higher states is imbalanced between electrons and holes. Applying a simple model in a nondegenerate limit, we can well describe the width dependence of the experimentally determined radiative rates. At room temperature, the decrease amounts to a factor of 2–4 for nonpolar quantum wells of 8 nm thickness.

DOI: [10.1103/PhysRevB.99.205308](https://doi.org/10.1103/PhysRevB.99.205308)**I. INTRODUCTION**

Radiative recombination processes in III-nitride quantum wells are usually governed by the built-in polarization fields, and the quantum-confined Stark effect [1] is a limiting factor for the radiative recombination of charge carriers [2]. Since electrons and holes are separated towards opposite sides of the quantum well, the oscillator strength drastically decreases with increasing quantum well width. On the contrary, quantum wells on nonpolar crystal orientations are free of polarization fields in the direction of growth [3] and provide an ideal basis for investigations of the radiative recombination processes in III-nitrides.

In order to increase the oscillator strength and the radiative emission, well widths of a few nanometers are common for polar quantum wells. For nonpolar orientations, thin quantum well widths (2–4 nm) can be found in the literature as well [4–8]. However, structures with larger well widths of 5–10 nm are also common [9–17], with a thickness up to 15 nm [18]. The increased quantum well widths are often found to be motivated in the context of possible applications like light-emitting devices. Here, the larger active volume and lower carrier densities might be beneficial to avoid high-order loss mechanisms like Auger recombination [19,20]. Furthermore, in nonpolar quantum wells the overlap of electron and hole wave functions is slightly larger for wide wells since the wave function penetration of the barrier is reduced. Although there exists some work reporting on better performance of structures with wide quantum wells [10,13], the dependence of the underlying recombination mechanisms on the quantum well width is often neglected.

Since structures with a variety of well widths are common, the width dependence of the radiative emission properties on nonpolar structures is investigated in this paper, focusing on

the basics of radiative recombination and the quantum well structure itself. The results show a substantial decrease of the radiative rate at room temperature for wide quantum wells due to fundamental selection rules, which is in agreement with a simple model calculation regarding the energies and populations of higher quantized valence band levels.

II. BASICS OF RADIATIVE RECOMBINATION

The quantum efficiency of light emission depends on radiative and nonradiative recombination processes in the structures. An improvement in the efficiency of a structure can be achieved by either reducing nonradiative recombination of charge carriers or enhancing the radiative recombination rates. Besides Auger recombination [19,21], nonradiative losses at defects acting as nonradiative recombination centers are a dominant factor [22–25]. Therefore, their reduction is pursued by using high-quality substrates or by improving the growth process itself [26,27].

In contrast, the radiative recombination processes are dominated by the physical properties of the semiconductor and the dimensionality of the structure. Assuming k conservation, the rate R_r of radiative band-to-band recombination for free electrons and holes in a direct-gap semiconductor can be described by [28]

$$R_r = Bnp, \quad (1)$$

with n and p being the electron and hole densities, respectively. The radiative recombination coefficient B itself is temperature dependent [29]:

$$B \propto T^{-d/2}, \quad (2)$$

with T being the temperature and d being the dimensionality of the system. In the case of III-N bulk material there is one conduction band and three valence bands (A, B, C), which show strongly polarized emission. Considering a two-dimensional (2D) system like a quantum well, the charge

* a.hangleiter@tu-bs.de

carriers get quantized and are restricted to certain energy levels in the conduction and valence bands. The quantized states are described by the index $m = 1, 2, 3, \dots$ for the conduction band and A_n, B_n, C_n , with $n = 1, 2, 3, \dots$, in the valence band. Since we focus on the general width dependence of the quantized states and not on the detailed valence band structure or polarization properties, we treat the valence bands regardless of their specific A, B, or C character and assume a single quantized state that is described by $n = 1, 2, 3, \dots$ instead of $A_1, B_1, C_1, A_2, \dots$. Each possible transition from the m th conduction band state to the n th valence band state will contribute to the total radiative rate R_r :

$$R_r = \sum_{m,n} R_{r,mn} = \sum_{m,n} B_{mn} n_m p_n, \quad (3)$$

where m, n denote the indices of the initial and final quantized states, respectively. Accordingly, the B coefficient for the radiative transition from the m th state in the conduction band to the n th state in the valence band of the quantum well can be written as [28]

$$B_{mn} = \frac{e^2 \tilde{n} \hbar \omega}{m_0^2 \epsilon_0 c^3 (m_e + m_h) k_B T} \langle |p_{CV}|^2 \rangle |M_{mn}|^2. \quad (4)$$

Here, e is the elementary charge, \tilde{n} is the refractive index, $\hbar\omega$ is the photon energy, m_0 is the electron mass, ϵ_0 is the vacuum permittivity, c is the speed of light, $m_{e,h}$ are the electron and hole effective masses, k_B is Boltzmann's constant, T is the temperature, $\langle |p_{CV}|^2 \rangle$ is the momentum matrix element for transitions from the conduction to the valence band, and $|M_{mn}|^2$ is the overlap matrix element of electron and hole envelope wave functions in the states with indices m and n . In the following, a theoretical description based on Eqs. (3) and (4) will be derived to describe the measured radiative rates. Therefore, the formation of excitons, the wave function overlap, and unequal thermal population of excited electron and hole states will be considered.

A. Wave function overlap

For a rectangular and symmetric potential well, each wave function $|\psi\rangle$ has a defined parity with respect to the quantum well center [30]. This assumption will be fulfilled by III-nitride quantum wells in nonpolar orientations, where no polarization fields are present in the direction of quantization [3]. The overlap matrix element of electron ($|\psi_m\rangle$) and hole ($|\psi_n\rangle$) wave functions is given by [30]

$$M_{mn} = \langle \psi_m | \psi_n \rangle. \quad (5)$$

The different transitions are illustrated in Fig. 1. In the limit of an infinite potential well only transitions with $\Delta n = n - m = 0$ are allowed, i.e., $|M_{mn}|^2 > 0$. In the more realistic case of a finite potential well weaker transitions, where $m + n$ is even, also become possible [30]. A numerical Schrödinger solver was used to estimate the magnitude of the overlap integral (see Fig. 2) in a nonpolar GaInN/GaN quantum well with a low InN mole fraction, which is comparable to the samples analyzed in this paper. The calculation parameters can be found in Table I. In Fig. 2 three different cases have to be distinguished: In the first case the wave functions have opposite parities ($m + n = \text{odd}$), and the overlap equals zero.

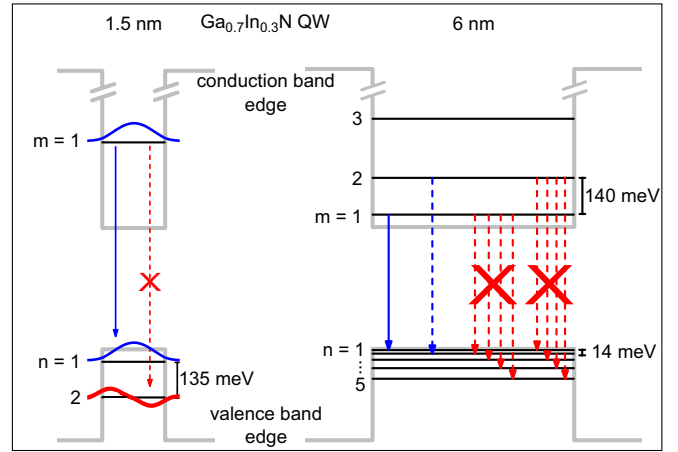


FIG. 1. Scheme showing allowed and forbidden transitions between the different quantized states in the conduction and valence bands. Exemplary energy separations are given for a thin (1.5 nm) QW and a thick (6 nm) QW. The given values for a GaInN/GaN QW with an exemplary indium content of $x_{\text{In}} = 30\%$ are based on numerical calculations using a Schrödinger solver with the parameters given in Table I.

In the second case the wave functions are equal in parity ($m + n = \text{even}$), but $m \neq n$ holds, which results in an overlap of $|M|^2 < 6\%$ that decreases rapidly with well width. This is low compared to the third case, where the overlap is near unity for $m = n$, or $\Delta n = 0$. Therefore, all transitions with $\Delta n \neq 0$ are neglected in a first approximation; that is, we set $R_r \approx R_{11} + R_{22} + \dots$, accepting a minor error in the theoretical description of the radiative rate.

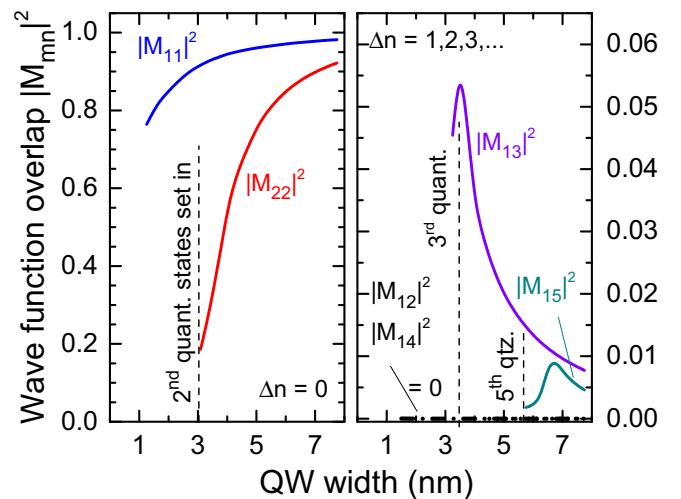


FIG. 2. Wave function overlaps between different states in the conduction and valence bands, with different scales for $\Delta n = 0$ (left) and $\Delta n \neq 0$ (right). Overlaps are plotted only in the width ranges where the respective quantized states are available in the QW, indicated by dashed lines. The given values are based on numerical calculations for a GaInN/GaN QW using a Schrödinger solver with the parameters given in Table I and an indium content of $x_{\text{In}} = 6\%$, which is comparable to the measured samples.

TABLE I. Basic parameters used for the numerical calculations with a Schrödinger solver. The GaInN values are linearly interpolated between those for GaN and InN according to the composition. For the band gap interpolation an additional bowing parameter is considered.

Parameter	GaN	InN
Effective electron mass [31]	$0.2m_0$	$0.07m_0$
Effective hole mass [31]	$2.0m_0$	$0.4m_0$
Band gap [32]	3.43 eV	0.69 eV
	GaInN	
Bowing parameter [31]	1.4 eV	
Band offset conduction band [33]	70% ΔE_g	
Band offset valence band [33]	30% ΔE_g	

B. Charge carrier density

In addition to the wave function overlap, the carrier densities in the initial and final states need to be regarded according to Eq. (3). For the large quantization energies in thin III-N quantum wells, mainly the states with $m, n = 1$ are populated at room temperature. This is illustrated in Fig. 1, which shows calculated data according to the parameters in Table I. Even if higher quantized states exist, the charge carriers' mean thermal energy ($k_B T \approx 26$ meV) is not sufficient to significantly overcome the energetic difference to the ground state, e.g., 135 meV in the valence band.

The situation is different for larger well widths, where the higher quantized states are shifted to smaller energies. This is particularly the case in the valence band with its large effective mass ($m_h = 2.0m_0$) compared to the conduction band ($m_e = 0.2m_0$) [31]. Therefore, the hole ground ($n = 1$) and excited states ($n \geq 2$) are separated by only 14 meV at 6-nm well width, and the excited hole states will get thermally occupied near room temperature ($p_n > 0$ for $n \geq 2$) since the higher states are in the range of $k_B T$. In contrast, electrons will stay in their lowest state ($n_1 \approx n$) since the electron ground and excited states are still separated by 140 meV for 6-nm well width. Given that higher electron states will not be occupied, even at room temperature and large well widths, we can assume that the ground-state transition, i.e., the transition from the lowest conduction band state to the highest valence band state ($m = 1 \rightarrow n = 1$), dominates the total radiative rate since other possible transitions have $\Delta n \neq 0$. Therefore, we assume $R_r \approx R_{r11}$.

The total error introduced by this approximation is still considered to be small since the product of a small overlap times low carrier densities is included in Eq. (3). As a consequence, the holes populating the excited states will not contribute to the radiative recombination due to the selection rule $\Delta n = 0$ and the unequally populated excited states, which will reduce the radiative rate significantly.

C. Reduced radiative emission

In order to estimate the reduction of the radiative rate, we need to quantify the fraction of holes in the ground state with respect to all possible states that can be occupied. In a nondegenerate limit, the population p_n of an excited hole state

can be described by Boltzmann statistics:

$$p_n = p_1 \exp\left(-\frac{\Delta E_n}{k_B T}\right), \quad (6)$$

where the energetic difference ΔE_n from the ground state ($n = 1$, with $\Delta E_1 = 0$ eV) depends on the width and depth of the potential well. Therefore, we obtain the ratio f_1 of holes in the ground state by summing over all valence band states:

$$f_1 \equiv \frac{p_1}{\sum_n p_n} = \frac{1}{\sum_n \exp\left(-\frac{\Delta E_n}{k_B T}\right)} \leq 1, \quad (7)$$

$$\Rightarrow R_r = B_{11} n p f_1. \quad (8)$$

Since $f_1 \leq 1$, the radiative rate will be reduced as soon as thermal occupation of excited hole states becomes significant. Up to now only the recombination of free electrons and holes, without the formation of excitons, has been considered. Even at room temperature, where excitons might thermally dissociate, earlier work showed that up to 60% of the charge carriers are bound into excitons [7,34,35]. For this reason, we extend our theoretical description by the recombination of excitons and apply the same considerations as above for free charge carriers. Thus, the product of charge carrier densities (np) in Eq. (1) is replaced by the exciton density x times the probability density of the electron-hole pair wave function at zero relative distance [36]:

$$R_x = B_{11} f_1 x |\psi(0)|^2 \quad (9)$$

$$= B_{11} f_1 x \frac{\pi a_B^2}{2} \equiv \frac{x}{\tau_x}. \quad (10)$$

Here, a_B is the free 2D exciton Bohr radius, and $\psi(0)$ is the exciton wave function for zero relative in-plane electron-hole distance. Experimentally, a reduction in the radiative rate can be measured as an increase in the (excitonic) radiative lifetime, which is given by [28,37]

$$\tau_x = \frac{\pi a_B^2}{2 B_{11} f_1}. \quad (11)$$

Therefore, we assume purely excitonic recombination as an approximation, which depends on temperature only via the B_{11} coefficient [see Eq. (4)]. The same T^1 dependence was found by Feldmann *et al.* [37] and Andreani *et al.* [38]. Even if excitons dissociate at elevated temperatures, which would introduce a superlinear rise of the radiative lifetime with temperature, the contribution should be the same for all investigated samples since the exciton binding energy varies only slightly over well width, as can be seen in Fig. 5 below from the width dependence of the exciton Bohr radius. Since only relative changes are considered for our analysis, we summarize the prefactors in Eq. (4) to a constant of proportionality C . This is justified since these factors are natural constants or vary only slightly with well width, e.g., the effective masses or the band gap. In fact, the calculated lifetimes would change by only 3% when considering an additional width dependence of the band gap. Instead, only the factors with a dominant dependence on quantum well width are considered in the following. After these simplifications, we end up with an excitonic radiative lifetime that depends on temperature T , the exciton Bohr radius a_B^2 , the overlap of electron and hole

wave functions of the ground state $|M_{11}|^2$, and the thermal population of excited hole states f_1 :

$$\tau_x = C \underbrace{\frac{T a_B^2}{|M_{11}|^2}}_{\tau_{x_0}} \frac{1}{f_1}. \quad (12)$$

Therefore, we introduce the lifetime τ_{x_0} , which is unaffected by effects of thermal population f_1 and depends only on temperature, exciton Bohr radius, and wave function overlap. Here, we find the temperature dependence that is explicitly included in Eq. (4) superimposed with that of f_1 , which will also depend on the quantum well's depth and width. Furthermore, we expect the overlap and the exciton Bohr radius to vary with the quantum well width.

To actually calculate the excitonic lifetime, Schrödinger's equation is solved numerically, using the parameters given in Table I. The sum over all Boltzmann terms is limited to $N = 100$:

$$f_1 = \left[\sum_{j=1}^N \exp\left(-\frac{\Delta E_j}{k_B T}\right) \right]^{-1}. \quad (13)$$

Between $N = 50$ and $N = 100$ the sum still increases by 5%, while higher valence band states ($N = 200$) increase the sum only by $<0.1\%$. To validate the above approximations we performed $6 \times 6 \mathbf{k} \cdot \mathbf{p}$ calculations using the approach described in Refs. [39,40]. The results are comparable to the simple model calculation above. In particular, the $\mathbf{k} \cdot \mathbf{p}$ calculations also show zero overlap for wave functions with opposite parity. Therefore, the transition rule $\Delta n = 0$ is found to be valid in a good approximation for our case. The calculated overlap values for other wave functions differ by only 1% from the simple calculations in the vicinity of the Γ point ($k = 0$). Larger deviations ($\approx 10\%$) are observed for the energies of the valence band levels, but the simple model is also able to reproduce the general width dependence of the quantized levels. Even though $\mathbf{k} \cdot \mathbf{p}$ calculations could give a more precise description of the valence band structure, the general trend of a reduced radiative emission with increasing well width would be unchanged. For simplicity, we prefer the simple model calculation with as few assumptions as possible.

Due to the decrease of ΔE with quantum well width, one has to expect a strong decrease in radiative recombination probability for larger well widths. This will result in an increased radiative carrier lifetime in the experiment. One should note that these considerations usually do not apply for (semi)polar quantum well structures, where the wave function symmetry is broken by the polarization fields and thus transitions with $\Delta n \neq 0$ also become possible. Nevertheless, the more prominent quantum-confined Stark effect will drastically decrease the radiative rates towards large well widths.

III. EXPERIMENTAL DETAILS

To demonstrate the impact of this effect experimentally, a series of nonpolar GaInN/GaN quantum well structures was prepared by low-pressure metalorganic vapor phase epitaxy (Aixtron AIX200RF). The four samples consist of an approximately 100-nm epitaxial GaN layer directly grown on *m*-plane

TABLE II. Overview of the samples under investigation, with quantum well (QW) width, InN mole fraction, emission wavelength at room temperature, and energetic difference of the valence band ground and first excited states.

Sample	QW width (nm)	x_{In} (%)	$\lambda(300 \text{ K})$ (nm)	ΔE_1 (meV)
A	1.3 ± 0.1	8.4 ± 1.9	369	42.4
B	2.3 ± 0.1	7.0 ± 0.6	381	42.3
C	3.8 ± 0.1	6.2 ± 0.4	387	23.9
D	6.3 ± 0.3	6.3 ± 0.6	390	10.2

pseudobulk GaN substrates (Kyma), followed by a threefold GaInN/GaN multiquantum well. The well width was varied between 1.25 and 6.25 nm, with a constant barrier thickness of 8 nm. To prevent relaxation at increasing thicknesses, a low InN mole fraction of $x_{\text{In}} = 6\%$ was chosen. The well width and InN mole fraction were determined using high-resolution x-ray diffractometry [41,42] (see details in Table II). Furthermore, all samples were found to be fully strained.

Time-resolved photoluminescence spectroscopy was performed using time-correlated single-photon counting (PicoQuant PicoHarp 3000). The sample temperature was varied between 5 and 300 K within a temperature-controlled helium bath cryostat. The samples were excited by 5-ps laser pulses at a wavelength of 350 nm and a repetition rate of 4 MHz using the second harmonic of a mode-locked and cavity-dumped dye laser beam (laser: Spectra-Physics Model 375, dye: Radiant Dyes Pyridine 2). The dye laser was optically pumped by the second harmonic of a synchronously mode-locked Nd:yttrium aluminum garnet laser (Spectra-Physics Model 3800S). The incident energy per pulse was approximately 5 nJ/cm^2 . A subtractive double-grating monochromator (Jobin Yvon, Spex 1680) in the Czerny-Turner configuration and a microchannel plate photomultiplier (Hamamatsu R3809U-02) were used to detect the dynamics of light emission down to decay times of 25 ps.

The transients of the intensity decay were collected in a spectral window of 16-20 nm around the emission maximum. The transient parameters I_0 (initial intensity) and τ (decay time) are obtained from single-exponential fits close to the initial part of the transient [43].

Generally, the decay time τ can be split into radiative (τ_r) and nonradiative (τ_{nr}) carrier lifetimes using the relation

$$\frac{1}{\tau} = \frac{1}{\tau_r} + \frac{1}{\tau_{\text{nr}}}. \quad (14)$$

Furthermore, the radiative lifetime is accessible by evaluating the temperature dependence of the inverse initial intensity $I_0(T)$, together with the initial decay time at low temperatures, where the recombination is considered purely radiative and the internal quantum efficiency becomes unity. Further details can be found in Ref. [43].

IV. RESULTS

A. Temperature dependence

The carrier lifetimes of all samples have a similar temperature dependence, as shown in Fig. 3 for sample B. The low-temperature decay times are around 500 ps at 5 K for all

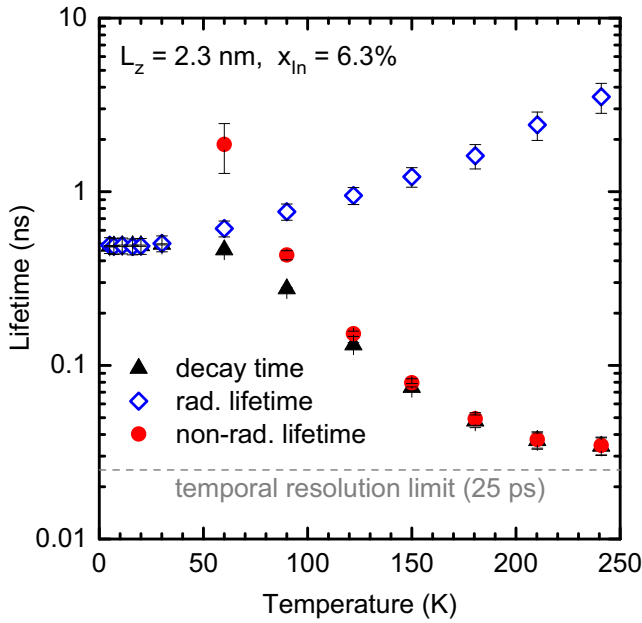


FIG. 3. Measured decay times and derived radiative and nonradiative lifetimes of sample B (2.3 nm thick, 6.3% indium content). The error bars contain the statistical uncertainties of the experiment and the evaluation process.

well widths. Up to ~ 30 K the recombination is dominated by localized charge carriers, indicated by the temperature-independent behavior of the radiative lifetime. This is consistent with the zero-dimensional case ($d = 0$) in Eq. (2), which yields a constant B coefficient of radiative recombination. The localization of carriers at potential minima is usually attributed to fluctuations in the quantum well width or InN mole fraction [44–48]. At higher temperatures, the charge carriers can escape the potential minima due to thermal

activation. This is the case for temperatures above 30 K, where the radiative lifetime starts to deviate from a constant behavior and the charge carriers have to be considered two-dimensional. In the range above 30 K the decay time also starts to decrease and is dominated by nonradiative recombination processes above 100 K. At the same time, the radiative lifetime begins to rise with temperature. Above 240 K the decay times approach the temporal resolution limit of 25 ps. For this reason, the measured decay times for higher temperatures are not reliable and will be omitted in the following analysis.

Concerning the relatively short nonradiative lifetimes observed in this sample series, a variety of nonradiative processes might be responsible. As described above, a low InN mole fraction is chosen for the samples to prevent relaxation at large well widths. This results in shallow potential wells, and thus, charge carrier escape over the barriers might play an important role. Former works also showed low nonradiative lifetimes for nonpolar quantum wells, which might be related to strain-induced defects like in the case of c -plane structures [43]. At least defects originating from the substrate should be negligible due to the high-quality bulk substrates used for the sample preparation. Also other thermally activated processes might contribute to the nonradiative rate and could probably be identified by determining activation energies from the temperature dependence of the nonradiative lifetimes. However, since in our analysis we focus on the radiative recombination, the discussion of nonradiative recombination mechanisms will be the subject of future work.

B. Well width dependence

The temperature-induced rise of the radiative lifetimes τ_r for samples of different well width is plotted in Fig. 4. The measured data and the calculated radiative lifetimes based on Eq. (12) for an InN mole fraction of 6% are given as a function of temperature. Most importantly, the theoretically

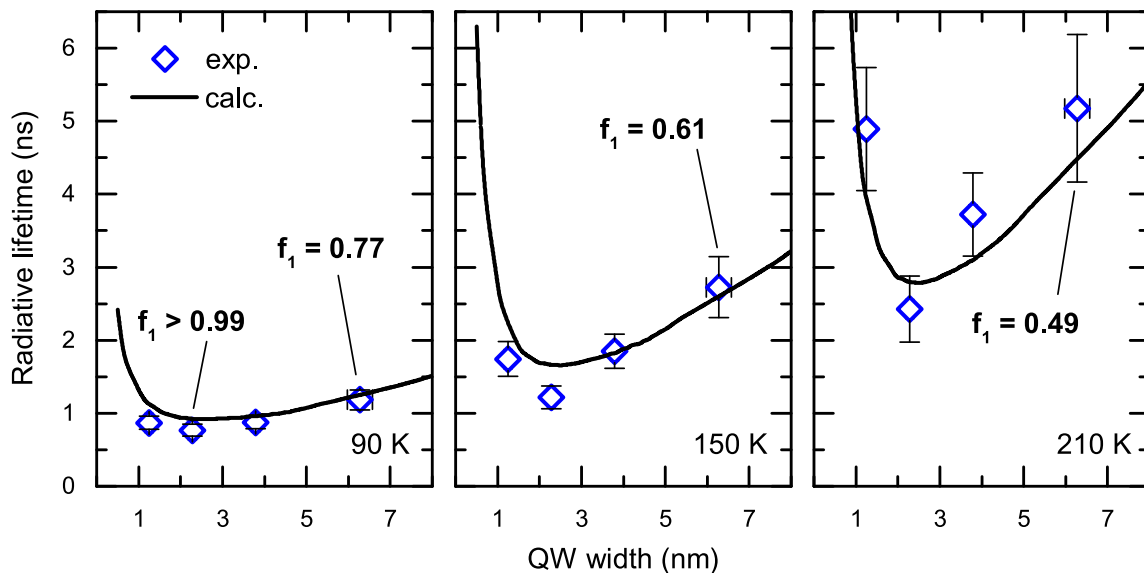


FIG. 4. Rise of radiative lifetimes with quantum well width; at higher temperatures the population of excited hole states dominates (indicated by a decreasing factor f_1) and results in a stronger increase in radiative lifetime. The curves calculated according to Eq. (12) are in good agreement with the experimental data.

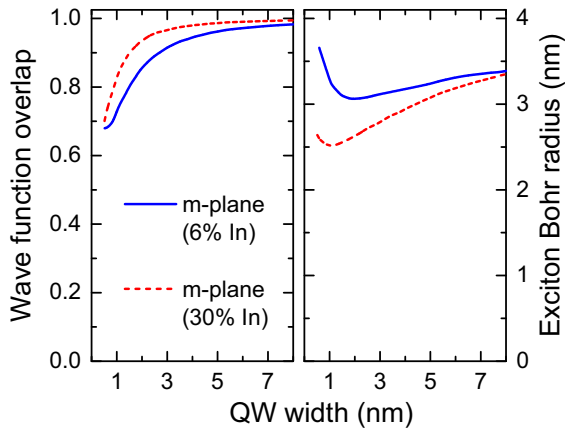


FIG. 5. Calculated wave function overlap $|M_{11}|^2$ and exciton Bohr radius a_B that vary only slightly over well width.

predicted rise of τ_r with quantum well width is confirmed by the measured data. Two regimes with different behaviors have to be distinguished in Fig. 4. At large well widths ($L_z > 2$ nm), we find a nearly linear increase of the radiative lifetimes. The slope of the curves is increasing with temperature and can be described by the calculations within the error margins. Equation (12) shows the dependencies of the calculated values, of which the wave function overlap, the exciton Bohr radius, and the fraction of holes remaining in the ground state depend on the well width. To clarify the single contributions, Fig. 5 shows the width dependence of $|M_{11}|^2$ and a_B^2 . For a low InN mole fraction (6%), overlap and exciton Bohr radius vary only slightly for wide wells and lead to a nearly constant excitonic radiative lifetime τ_{x_0} , as shown in Fig. 6. The linear rise that can be observed in the measurements is reproduced only when we account for the thermal population of excited valence band states for τ_x . In contrast, the lifetime τ_{x_0} , which depends only on temperature, exciton Bohr radius, and wave function overlap [see Eq. (12)], does not show the steep increase for

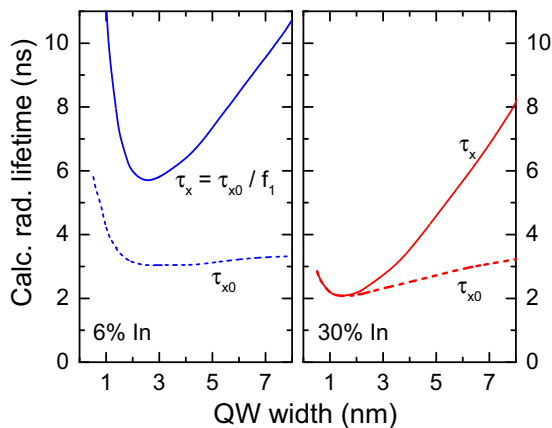


FIG. 6. Calculated radiative lifetimes at room temperature (300 K) according to Eq. (12), where τ_{x_0} (dashed line) depends only on temperature, overlap, and exciton Bohr radius, while τ_x (solid line) includes the factor f_1 to account for the population of excited valence band states.

larger well widths that is observed experimentally. Therefore, the charge carrier behavior in this regime is clearly dominated by a reduced population of the hole ground state.

In the regime of very thin quantum wells ($L_z \leq 2$ nm), an increase in the measured radiative lifetimes can be observed in Fig. 4 as well. Here, the rise is mainly related to a decreasing overlap and exciton binding energy in this regime, where electron and hole wave functions already penetrate into the barriers. This is emphasized by the data shown in Fig. 5. These contributions are expected to be independent of the depth of the potential well and its InN mole fraction. Especially for samples with shallow potential wells, like in our case with $x_{\text{In}} = 6\%$, we expect an additional contribution to the rising lifetimes. Here, the increasing quantization for thin wells shifts the hole ground state towards the edge of the potential well, where the excited states are accumulating. This reduces the effective energy difference between ground and excited states and again makes their thermal population possible. Also the transition to three-dimensional bulk states might be in the range of thermal activation. Hence, the reduced ground-state population also has an impact at very thin well widths and low InN mole fractions. This contribution is negligible for higher InN mole fractions and larger band discontinuities, as can be seen in Fig. 6, where both calculated curves for $x_{\text{In}} = 30\%$ merge at decreasing thickness. Remarkably, the overall radiative lifetimes are lower for the higher InN mole fraction, and consequently, the relative increase in radiative lifetimes is higher. The curves in Fig. 6 show an increase in calculated lifetimes by a factor of 3.9 for a high InN mole fraction and a factor of 1.9 for a low InN mole fraction for a width range up to 8 nm and at a temperature of 300 K.

This significant increase in radiative lifetime can also be observed in the measured data, where the width dependence of τ_r is measurable already at 90 K, where τ_r is dominated by wave function overlap and the exciton Bohr radius. The linear increase gets steeper for 150 and 210 K, where the radiative lifetimes are clearly dominated by the effect of thermally populated excited hole states. Although only a limited temperature range is accessible in our experiments, an increase by a factor of 2 in the radiative lifetime is demonstrated experimentally in the width range between 2 and 6 nm (samples B–D), which coincides with the calculated value (factor of 1.9). The observed increase in radiative lifetime corresponds to a decrease in the radiative rate by 50%. This effect will be even more prominent at higher temperatures and larger InN mole fractions. The increase in radiative lifetime towards thin quantum wells becomes important only for very low InN mole fractions.

V. CONCLUSION

In summary, our results show a significant decrease of the radiative rate for wide quantum wells on nonpolar *m*-plane substrates. Basically, this trend should be present in all III-N materials in nonpolar growth directions since it originates from the selection rule $\Delta n = 0$, combined with the unequal population of higher electron and hole quantized states. The considerations will also apply for the recombination of free electrons and holes instead of excitons, which were included in our analysis. As a consequence, the use of wide quantum

wells is not favorable, which was also reported in earlier work [49], where the better performance of nonpolar structures with thin quantum wells was assigned to the wave function overlap and the exciton binding energy, leaving out the impact of selection rules and the population of excited states. Besides that, for an overall high internal quantum efficiency the nonradiative rate should be minimized for thin quantum wells as well. Generally, we do not expect that nonradiative

processes are stronger in thin quantum wells, although we suspect carrier escape into the barriers is an important factor for shallow potential wells. This, of course, depends strongly on the nature of the nonradiative recombination process and therefore will be the subject of future work. Still, the strong width dependence of the radiative rate should be considered when designing light emitters based on nonpolar III-N structures.

-
- [1] T. Takeuchi, S. Sota, M. Katsuragawa, M. Komori, H. Takeuchi, H. Amano, and I. Akasaki, *Jpn. J. Appl. Phys.* **36**, L382 (1997).
- [2] J. S. Im, H. Kollmer, J. Off, A. Sohmer, F. Scholz, and A. Hangleiter, *Phys. Rev. B* **57**, R9435 (1998).
- [3] P. Waltereit, O. Brandt, A. Trampert, H. T. Grahn, J. Menniger, M. Ramsteiner, M. Reiche, and K. H. Ploog, *Nature (London)* **406**, 865 (2000).
- [4] Y. J. Sun, O. Brandt, S. Cronenberg, S. Dhar, H. T. Grahn, K. H. Ploog, P. Waltereit, and J. S. Speck, *Phys. Rev. B* **67**, 041306(R) (2003).
- [5] V. Liuolia, S. Marcinkevičius, Y.-D. Lin, H. Ohta, S. P. DenBaars, and S. Nakamura, *J. Appl. Phys.* **108**, 023101 (2010).
- [6] D. Sutherland, T. Zhu, J. T. Griffiths, F. Tang, P. Dawson, D. Kundy, F. Oehler, M. J. Kappers, C. J. Humphreys, and R. A. Oliver, *Phys. Status Solidi B* **252**, 965 (2015).
- [7] W. Liu, R. Butté, A. Dussaigne, N. Grandjean, B. Deveaud, and G. Jacopin, *Phys. Rev. B* **94**, 195411 (2016).
- [8] T. Zhu, D. Gachet, F. Tang, W. Y. Fu, F. Oehler, M. J. Kappers, P. Dawson, C. J. Humphreys, and R. A. Oliver, *Appl. Phys. Lett.* **109**, 232103 (2016).
- [9] T. Onuma, A. Chakraborty, B. A. Haskell, S. Keller, S. P. DenBaars, J. S. Speck, S. Nakamura, U. K. Mishra, T. Sota, and S. F. Chichibu, *Appl. Phys. Lett.* **86**, 151918 (2005).
- [10] K.-C. Kim, M. C. Schmidt, H. Sato, F. Wu, N. Fellows, Z. Jia, M. Saito, S. Nakamura, S. P. DenBaars, J. S. Speck, and K. Fujito, *Appl. Phys. Lett.* **91**, 181120 (2007).
- [11] S. Marcinkevičius, K. M. Kelchner, S. Nakamura, S. P. DenBaars, and J. S. Speck, *Appl. Phys. Lett.* **102**, 101102 (2013).
- [12] S. Marcinkevičius, K. M. Kelchner, L. Y. Kuritzky, S. Nakamura, S. P. DenBaars, and J. S. Speck, *Appl. Phys. Lett.* **103**, 111107 (2013).
- [13] N. A. Pfaff, K. M. Kelchner, D. F. Feezell, S. Nakamura, S. P. DenBaars, and J. S. Speck, *Appl. Phys. Express* **6**, 092104 (2013).
- [14] S. Marcinkevičius, K. M. Kelchner, S. Nakamura, S. P. DenBaars, and J. S. Speck, *Phys. Status Solidi C* **11**, 690 (2014).
- [15] M. Shahmohammadi, W. Liu, G. Rossbach, L. Lahourcade, A. Dussaigne, C. Bougerol, R. Butté, N. Grandjean, B. Deveaud, and G. Jacopin, *Phys. Rev. B* **95**, 125314 (2017).
- [16] R. Ivanov, S. Marcinkevičius, T. K. Uždavinys, L. Y. Kuritzky, S. Nakamura, and J. S. Speck, *Appl. Phys. Lett.* **110**, 031109 (2017).
- [17] R. Ivanov, S. Marcinkevičius, M. D. Mensi, O. Martinez, L. Y. Kuritzky, D. J. Myers, S. Nakamura, and J. S. Speck, *Phys. Rev. Appl.* **7**, 064033 (2017).
- [18] Y. Huang, K. W. Sun, A. M. Fischer, Q. Y. Wei, R. Juday, F. A. Ponce, R. Kato, and T. Yokogawa, *Appl. Phys. Lett.* **98**, 261914 (2011).
- [19] Y. C. Shen, G. O. Mueller, S. Watanabe, N. F. Gardner, A. Munkholm, and M. R. Krames, *Appl. Phys. Lett.* **91**, 141101 (2007).
- [20] Y.-L. Li, Y.-R. Huang, and Y.-H. Lai, *Appl. Phys. Lett.* **91**, 181113 (2007).
- [21] M. Brendel, A. Kruse, H. Jönen, L. Hoffmann, H. Bremers, U. Rossow, and A. Hangleiter, *Appl. Phys. Lett.* **99**, 031106 (2011).
- [22] T. Sugahara, H. Sato, M. Hao, Y. Naoi, S. Kurai, S. Tottori, K. Yamashita, K. Nishino, L. T. Romano, and S. Sakai, *Jpn. J. Appl. Phys.* **37**, L398 (1998).
- [23] K. Saarinen, T. Laine, S. Kuisma, J. Nissilä, P. Hautojärvi, L. Dobrzynski, J. M. Baranowski, K. Pakula, R. Stepniewski, M. Wojdak, A. Wyszomolek, T. Suski, M. Leszczynski, I. Grzegory, and S. Porowski, *Phys. Rev. Lett.* **79**, 3030 (1997).
- [24] A. Uedono, S. F. Chichibu, Z. Q. Chen, M. Sumiya, R. Suzuki, T. Ohdaira, T. Mikado, T. Mukai, and S. Nakamura, *J. Appl. Phys.* **90**, 181 (2001).
- [25] S. F. Chichibu, A. Uedono, T. Onuma, T. Sota, B. A. Haskell, S. P. DenBaars, J. S. Speck, and S. Nakamura, *Appl. Phys. Lett.* **86**, 021914 (2005).
- [26] H. Amano, N. Sawaki, I. Akasaki, and Y. Toyoda, *Appl. Phys. Lett.* **48**, 353 (1986).
- [27] S. Nakamura, M. Senoh, S. Nagahama, N. Iwasa, T. Yamada, T. Matsushita, H. Kiyoku, Y. Sugimoto, T. Kozaki, H. Umemoto, M. Sano, and K. Chocho, *Jpn. J. Appl. Phys.* **37**, L627 (1998).
- [28] P. K. Basu, *Theory of Optical Processes in Semiconductors: Bulk and Microstructures, Series on Semiconductor Science and Technology* (Clarendon, Oxford, 1997).
- [29] P. T. Landsberg, *Recombination in Semiconductors* (Cambridge University Press, Cambridge, 1991).
- [30] G. Bastard, *Wave Mechanics Applied to Semiconductor Heterostructures, Monographies de physique* (Editions de Physique, Les Ulis, France, 1996).
- [31] I. Vurgaftman and J. R. Meyer, *J. Appl. Phys.* **94**, 3675 (2003).
- [32] J. Wu, W. Walukiewicz, W. Shan, K. M. Yu, J. W. Ager, S. X. Li, E. E. Haller, H. Lu, and W. J. Schaff, *J. Appl. Phys.* **94**, 4457 (2003).
- [33] G. Martin, A. Botchkarev, A. Rockett, and H. Morko, *Appl. Phys. Lett.* **68**, 2541 (1996).
- [34] A. Hangleiter, Z. Jin, M. Gerhard, D. Kalincev, T. Langer, H. Bremers, U. Rossow, M. Koch, M. Bonn, and D. Turchinovich, *Phys. Rev. B* **92**, 241305(R) (2015).

- [35] T. Langer, A. Chernikov, D. Kalincev, M. Gerhard, H. Bremers, U. Rossow, M. Koch, and A. Hangleiter, *Appl. Phys. Lett.* **103**, 202106 (2013).
- [36] R. J. Elliott, *Phys. Rev.* **108**, 1384 (1957).
- [37] J. Feldmann, G. Peter, E. O. Göbel, P. Dawson, K. Moore, C. Foxon, and R. J. Elliott, *Phys. Rev. Lett.* **59**, 2337 (1987).
- [38] L. C. Andreani, F. Tassone, and F. Bassani, *Solid State Commun.* **77**, 641 (1991).
- [39] W. G. Scheibenzuber, U. T. Schwarz, R. G. Veprek, B. Witzigmann, and A. Hangleiter, *Phys. Rev. B* **80**, 115320 (2009).
- [40] S. L. Chuang and C. S. Chang, *Phys. Rev. B* **54**, 2491 (1996).
- [41] H. Bremers, A. Schwiegel, L. Hoffmann, H. Jönen, U. Rossow, J. Thalmer, J. Zweck, and A. Hangleiter, *Phys. Status Solidi B* **248**, 616 (2010).
- [42] H. Jönen, H. Bremers, U. Rossow, T. Langer, A. Kruse, L. Hoffmann, J. Thalmer, J. Zweck, S. Schwaiger, F. Scholz, and A. Hangleiter, *Semicond. Sci. Technol.* **27**, 024013 (2012).
- [43] T. Langer, H. Jönen, A. Kruse, H. Bremers, U. Rossow, and A. Hangleiter, *Appl. Phys. Lett.* **103**, 022108 (2013).
- [44] N. Grandjean, B. Damilano, and J. Massies, *J. Phys.: Condens. Matter* **13**, 6945 (2001).
- [45] S. Dhar, U. Jahn, O. Brandt, P. Waltereit, and K. Ploog, *Phys. Status Solidi A* **192**, 85 (2002).
- [46] D. M. Graham, A. Soltani-Vala, P. Dawson, M. J. Godfrey, T. M. Smeeton, J. S. Barnard, M. J. Kappers, C. J. Humphreys, and E. J. Thrush, *J. Appl. Phys.* **97**, 103508 (2005).
- [47] D. Watson-Parris, M. J. Godfrey, P. Dawson, R. A. Oliver, M. J. Galtrey, M. J. Kappers, and C. J. Humphreys, *Phys. Rev. B* **83**, 115321 (2011).
- [48] T. Schulz, T. Remmele, T. Markurt, M. Korytov, and M. Albrecht, *J. Appl. Phys.* **112**, 033106 (2012).
- [49] G. A. Garrett, H. Shen, M. Wraback, A. Tyagi, M. C. Schmidt, J. S. Speck, S. P. DenBaars, and S. Nakamura, *Phys. Status Solidi C* **6**, S800 (2009).